

Intrinsic interface exchange coupling of ferromagnetic nanodomains in a charge ordered manganite

D. Niebieskikwiat and M.B. Salamon

*Department of Physics and Frederick Seitz Materials Research Laboratory,
University of Illinois at Urbana-Champaign, Urbana, Illinois 61801, USA*

We present a detailed magnetic study of the $\text{Pr}_{1/3}\text{Ca}_{2/3}\text{MnO}_3$ manganite, where we observe the presence of small ferromagnetic (FM) domains (diameter ~ 10 Å) immersed within the charge-ordered antiferromagnetic (AFM) host. Due to the interaction of the FM nanodroplets with a disordered AFM shell, the low-temperature magnetization loops present exchange bias (EB) under cooling in an applied magnetic field. Our analysis of the cooling field dependence of the EB yields an antiferromagnetic interface exchange coupling comparable to the bulk exchange constant of the AFM phase. We also observe training effect of the EB, which is successfully described in terms of a preexisting relaxation model developed for other classical EB systems. This work provides the first evidence of intrinsic interface exchange coupling in phase separated manganites.

PACS numbers: 75.60.-d, 75.30.Gw, 75.70.Cn, 75.47.Lx

I. INTRODUCTION

The search for improved materials for magnetic recording and permanent magnets has been the driving force for research work in the area of magnetic condensed matter physics.¹ Artificially exchange-biased systems, like ferromagnetic-antiferromagnetic (FM-AFM) multilayers, have been widely studied, and they have been shown to provide large saturation magnetizations (M_S) as well as high coercive fields (H_C).¹ However, the usually small exchange bias field (H_E) is ultimately limited by the ability of the system to create an uncompensated magnetization at the antiferromagnet interface (m_i).^{1,2,3,4,5} This interfacial magnetic moment induces a unidirectional anisotropy on the ferromagnet, and depends on a number of parameters including disorder, AFM domain- and domain-wall-size, surface roughness, etc.^{6,7,8,9} A different kind of system, known as exchange-spring magnet was proposed by Skomski and Coey¹⁰ to provide a rather large exchange anisotropy energy. In two-phase nanocomposites, small soft-FM inclusions adopt the anisotropy energy of a hard-FM matrix. Such a case was observed in $\text{Nd}_2\text{Fe}_{14}\text{B}/\alpha\text{-Fe}$ alloys.¹¹ Similarly, exchange anisotropy interactions have been studied in another large group of inhomogeneous materials presenting FM-AFM interfaces, like Fe/Fe-oxide,^{12,13} Co/CoO,^{2,14} and Ni/NiO¹⁵ nanocomposites, spin glasses, etc.¹

In the heavily studied manganites, inhomogeneous magnetic phases are known to be at the root of the colossal magnetoresistance effect.¹⁶ Considering the presence of FM-AFM interfaces, exchange anisotropy interactions can also be expected in these materials. However, we are not aware of any study of interface exchange anisotropy in inhomogeneous manganites so far. In this paper, we present a meticulous magnetic study of the $\text{Pr}_{1/3}\text{Ca}_{2/3}\text{MnO}_3$ manganite, and show clear signatures of interface exchange coupling of FM nanodomains immersed in the AFM background. Through an analysis of the shift of the magnetization loops at low temperatures,

we find that the surface exchange interaction is of AFM nature, and its magnitude is similar to the bulk exchange interaction within the AFM volume. Finally, we also observe a training effect of the exchange bias, which is successfully analyzed using an existing relaxation model.

II. EXPERIMENT

The polycrystalline $\text{Pr}_{1/3}\text{Ca}_{2/3}\text{MnO}_3$ compound was prepared by the nitrate decomposition route, as described elsewhere,¹⁷ from high purity Pr_6O_{11} , CaCO_3 , and MnO . The final sintering process was made at 1500 °C for 24 h, after which the sample was slowly cooled to room temperature.

Magnetization (M) measurements were performed in a Superconducting Quantum Interference Device (SQUID) magnetometer with applied magnetic fields H up to 70 kOe in the temperature range $5 \text{ K} \leq T \leq 350 \text{ K}$. The temperature dependence of the magnetization was measured on warming with an applied field $H = 10$ kOe, in both field-cooling (FC) and zero-field-cooling (ZFC) processes.

III. RESULTS AND DISCUSSION

A. Observation of phase coexistence and exchange anisotropy

Figure 1 presents data of M/H as a function of temperature for the $\text{Pr}_{1/3}\text{Ca}_{2/3}\text{MnO}_3$ manganite. The physical properties of this compound are mainly determined by the electrons on the Mn ions. There is a Mn core, where three electrons are strongly coupled to a total spin $3/2$. The $\text{Pr}^{3+}/\text{Ca}^{2+}$ ratio introduces one doping electron for every three Mn sites, responsible for the electrical transport. The peak of M/H at $T_{CO} \approx 273 \text{ K}$ indicates the charge ordering transition of the material,^{18,19} where the double exchange interaction is suppressed due

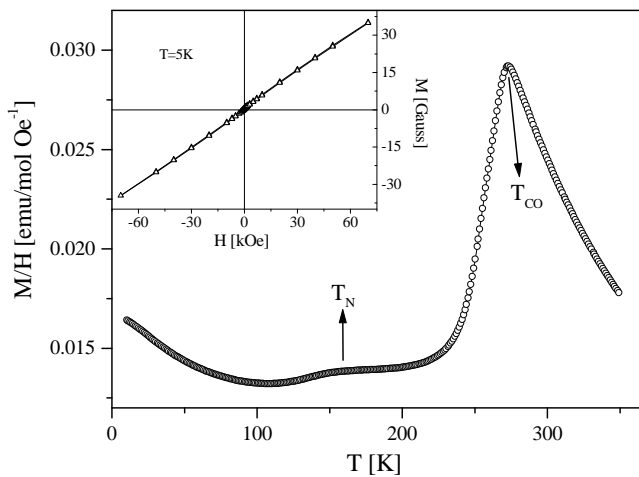


FIG. 1: Susceptibility (M/H) of the $\text{Pr}_{1/3}\text{Ca}_{2/3}\text{MnO}_3$ compound as a function of temperature ($H = 10$ kOe). Inset: M - H loop at $T = 5$ K, after field cooling the sample from 300 K with $H_{cool} = 70$ kOe.

to the localization of the charge carriers, producing a large drop of the susceptibility. At a lower temperature, the charge-ordered phase undergoes a paramagnetic-to-antiferromagnetic transition at $T_N \approx 155$ K.^{18,19} The inset of Fig. 1 shows the linear $M(H)$ curve of the AFM phase at $T = 5$ K. However, even though the overall M - H response is as expected, the sample exhibits some peculiar behavior when is cooled with an applied magnetic field. The curve in the inset of Fig. 1 was measured after cooling the sample from 300 K to 5 K with an applied cooling field $H_{cool} = 70$ kOe. A more careful examination of these data reveals two notable features, namely a hysteresis (coercivity) and a shift of the $M(H)$ curve from the origin, i.e. exchange bias. It is worth mentioning that the shift of the loops has the same magnitude but opposite sign when the cooling field is negative, confirming the existence of the exchange bias phenomenon. For $H_{cool} = 0$ the exchange bias effect goes away, while the still-present coercivity is greatly reduced.

The two features clearly indicate that, superposed on the predominant AFM signal, there is a minor FM component showing the presence of small FM inclusions. This FM component becomes evident in Fig. 2, where we present the resulting magnetization (M^*) after the AFM moment is subtracted. This intrinsic coexistence of different magnetic phases is commonly found in many manganese perovskite compounds in the whole range of carrier doping, and is usually referred to as electronic phase separation.^{16,17,18}

As the magnetic field is reduced from the maximum value 70 kOe, the ferromagnetic moment becomes negative at $H_1 \sim -3.8$ kOe, while on the increasing branch of the loop M^* changes sign at $H_2 \sim -0.5$ kOe. These two fields define a coercive field $H_C = (H_2 - H_1)/2 \sim 1.6$ kOe and an exchange bias field $H_E = (H_2 + H_1)/2 \sim -2.1$

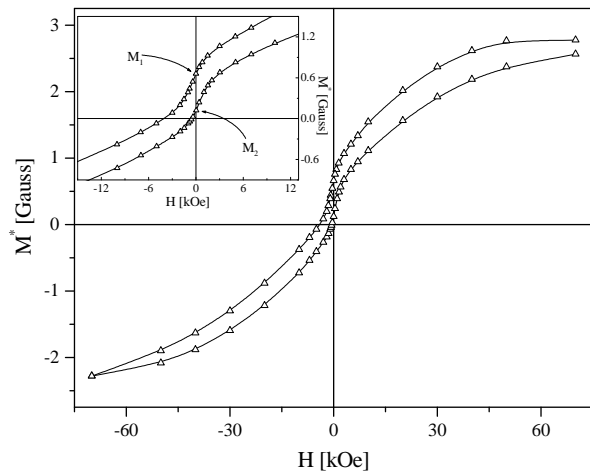


FIG. 2: Resulting magnetization (M^*) vs H loop, after subtracting the contribution of the AFM matrix ($T = 5$ K, $H_{cool} = 70$ kOe). Inset: blow-up of the low-field region, showing the determination of the remanent moments M_1 and M_2 .

kOe. However, the values of H_1 and H_2 depend on the value of the susceptibility used to subtract the AFM background, thus preventing a precise determination of H_E . Alternatively, the exchange bias behavior can be seen as a vertical shift of the $M^*(H)$ loop, as evidenced by the positive remanent magnetization obtained even after recoil from a very negative reverse field (-70 kOe). This effect is a manifestation of the presence of a unidirectional exchange anisotropy interaction, which drives the FM domains back to the original orientation when the magnetic field is removed. Therefore, since for $H = 0$ there is no contribution from the AFM volume, we choose to quantify the exchange bias effect using the remanent magnetization. For this reason, we define the magnetization shift M_E and the magnetic coercivity M_C as the “vertical axis” equivalents of H_E and H_C , respectively. Naming as M_1 and M_2 the remanent magnetizations on the field decreasing and increasing branches of the loop, respectively (as in the inset of Fig. 2), we define $M_C = (M_1 - M_2)/2$ and $M_E = (M_1 + M_2)/2$ (for the data shown in Fig. 2, $M_C \approx 0.26$ Gauss and $M_E \approx 0.40$ Gauss). With these definitions, M_C and M_E are quantitative indications of coercivity and exchange bias, respectively. Indeed, in the simplest model of single-domain FM particles (that we assume in this work), a relationship between M_E and H_E can be easily derived. Considering the magnetic moments switching by thermal activation over the anisotropy barrier KV (K is the anisotropy constant and V the volume of the particles), the exchange bias field introduces an asymmetry in the activation energy for the backward and forward switching such that

$$\frac{M_E}{M_S} \sim -2\nu_o\tau e^{-\frac{KV}{k_B T}} \sinh\left(\frac{\mu H_E}{k_B T}\right) \quad (1)$$

where M_S is the saturation magnetization, $\nu_o \sim 10^9 \text{ sec}^{-1}$ is the switching attempt frequency, $\tau \sim 10^2 - 10^3 \text{ sec}$ is the typical measurement time, k_B is the Boltzmann constant, and μ is the magnetic moment of the FM particles. For a small enough magnetic energy ($\mu H_E < k_B T$), Eq. (1) can be rewritten as

$$\frac{M_E}{M_S} \propto -H_E \quad (2)$$

indicating a direct equivalence between M_E and H_E . Our analysis in the next subsection shows that $\mu H_E / k_B T$ is always lower than 0.9, justifying *a posteriori* the use of this relationship.

B. Origin of the exchange anisotropy: temperature and cooling-field dependence

The fact that reverse fields as high as -70 kOe are not able to produce a negative M_2 , indicates that the exchange interactions giving rise to the described effects must be of considerable strength. The origin of such exchange anisotropy is revealed by the temperature dependence of the magnetization shift, as presented in Fig. 3. In this case, the sample was cooled down from 300 K to 5 K with an applied field $H_{cool} = 50 \text{ kOe}$, and warmed back to the measuring temperature without removing the applied field. At the appropriate temperature, the magnetization loop was measured between 50 and -50 kOe , from which M_E and M_C were calculated. It can be seen that, as the temperature increases, the magnetization shift vanishes right at the Néel temperature of the AFM background, $T_N \sim 155 \text{ K}$, while the coercivity remains present up to the temperature marked as T_0 , which is $\sim 30 \text{ K}$ higher than T_N and indicates the onset of the FM component.

The temperature evolution shown in Fig. 3 is typical of exchange bias systems.^{1,2,3,4,5,6,7,8,9} As the sample is cooled through T_N with an applied magnetic field, the exchange interaction between the AFM phase and the polarized FM phase induces an interface magnetic moment on the antiferromagnet (m_i), which remains frozen at lower temperatures.^{3,4,20} In turn, below the freezing temperature T_f ($\leq T_N$), m_i provides the necessary pinning forces (exchange anisotropy) to drive the ferromagnet back to a positive remanence on recoil. Then, the exchange bias behavior, observed through the appearance of a distinctive magnetization shift, is induced by the interface exchange coupling between the FM domains and the charge-ordered AFM background.

Although the magnetization shift first develops at $T_N \approx 155 \text{ K}$, it is useful to note that the main freezing temperature of the system is $T_f \sim 35 \text{ K}$. The inset of Fig. 3 shows the temperature dependence of the ratio M_{FC}/M_{ZFC} , the magnetization of the material measured in FC and ZFC processes, respectively. The increase of this ratio below T_f is due to the enhancement

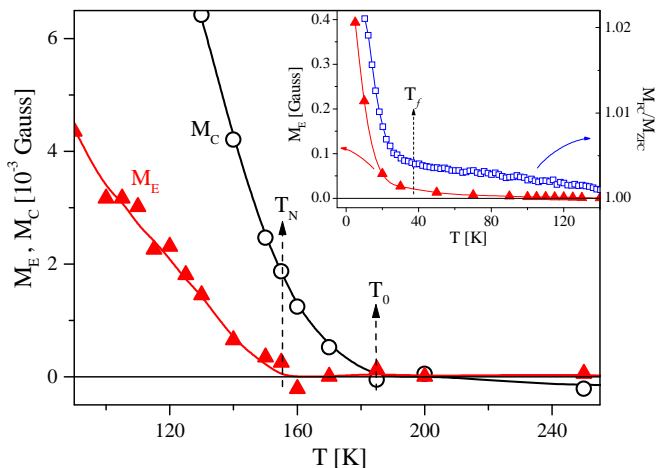


FIG. 3: Temperature dependence of M_E and M_C , showing the onset of exchange bias and coercivity at T_N and T_0 , respectively. Inset: M_E and the ratio M_{FC}/M_{ZFC} at low temperatures. Both quantities sharply increase below the freezing temperature, $T_f \sim 35 \text{ K}$.

of the magnetic irreversibility induced by the freezing of the surface spins. Simultaneous with the upward turn of M_{FC}/M_{ZFC} , M_E also exhibits a steep increase of more than one order of magnitude below $\sim 35 \text{ K}$. This indicates that a small number of interfaces start to freeze at T_N , but the dominant contribution to the low temperature M_E comes from domains with $T_f \sim 35 \text{ K}$. The existence of low- T_f spins has been also observed in other systems,^{3,12,13,21,22,23} and have been attributed to glass-like phases occurring in spin-disordered surfaces around the ordered particles.^{12,13,21,22} Indeed, the irreversibility shown by the ratio M_{FC}/M_{ZFC} is a fingerprint of the glassy behavior in nanoparticles systems. In this context, a partial alignment of the glassy spins leads to the interface moment m_i , and the temperature T_f is a measure of the energy barriers separating multiple spin configurations of the glass-like phase.

In order to get some insight into the properties of this exchange biased system, we studied the cooling field dependence of M_E . For each data point shown in Fig. 4, the sample was cooled from 300 K to 5 K with the applied cooling field, and a hysteresis loop was measured between 70 and -70 kOe . As shown in this figure, M_E presents a smooth increasing dependence with H_{cool} , which saturates at high cooling fields.

The exchange bias field is usually thought as the balance between the Zeeman energy of the FM particles and the surface energy due to the interface exchange interaction,^{2,6} i.e.,

$$N_v g \mu_B H_E = -N_i J_i \frac{m_i}{g \mu_B} \quad (3)$$

N_v and N_i are the number of spins inside the FM volume and on the disordered AFM shell, respectively, thus

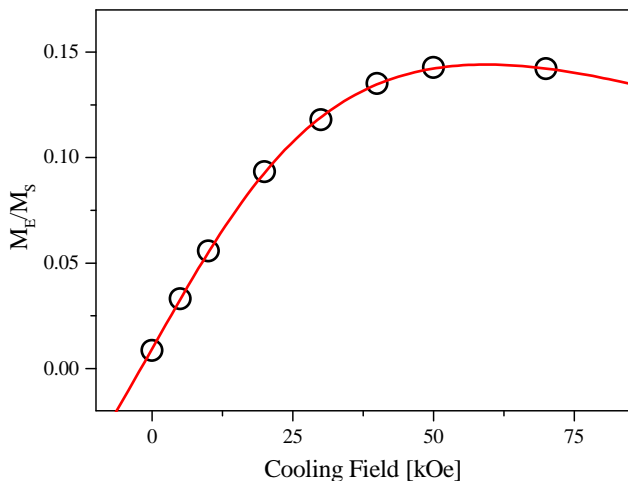


FIG. 4: Cooling field dependence of M_E . The solid line is a fit with an exchange interaction model between the FM domains and a disordered AFM shell (see text).

H_E depends, as expected, on the surface-to-volume ratio. The surface exchange constant is represented by J_i , $g \approx 2$ is the gyromagnetic factor, and μ_B is the Bohr magneton. From Eq. (3), the usual Meiklejohn-Bean expression² for FM-AFM bilayers is easily recovered by making the appropriate replacements, e.g. $N_i/N_v \rightarrow a/t_F$, where a is the out-of-plane lattice parameter and t_F the thickness of the FM layer.

For small cooling fields, the coupling of the interface moment to the FM volume dominates over the coupling of m_i to H_{cool} , implying that the surface spin configuration minimizes the surface energy and $J_i m_i > 0$, producing a negative H_E . However, it has been shown that for AFM couplings ($J_i < 0$), a large enough cooling field could prevail and flip the interface moment, producing a positive m_i at the freezing temperature and changing the sign of the exchange bias field.²⁴ Assuming 1-to-1 core-shell spin interactions, these competing energies can be described in an effective magnetic field acting on the interface moment during the freezing process as

$$H_{ef} = \frac{J_i}{(g\mu_B)^2} m_F(T_f) + H_{cool} \quad (4)$$

with $m_F(T_f)$ the magnetic moment per FM spin at the freezing temperature. For our small magnetic domains, we assume $m_F(T_f) = \mu_o L(x)$, where $\mu_o \approx 3 \mu_B$ is the magnetic moment of the Mn core spin, $L(x)$ is the Langevin function, $x = \mu H_{cool}/k_B T_f$, and $\mu = N_v \mu_o$. At lower temperatures, because of the glassy behavior of the surface spins the interface moment $m_i (\propto H_{ef})$ remains frozen, inducing the exchange bias response. Therefore, combining Eqs. (2), (3), and (4) we obtain

$$-H_E \propto \frac{M_E}{M_S} \propto J_i \left[\frac{J_i \mu_o}{(g\mu_B)^2} L \left(\frac{\mu H_{cool}}{k_B T_f} \right) + H_{cool} \right] \quad (5)$$

In this equation, the competition between the exchange interaction and the cooling field becomes evident. For small H_{cool} the first term usually dominates, and $H_E (< 0)$ depends on J_i^2 . However, for large cooling fields the second term ($\propto J_i$) becomes important, and for $J_i < 0$ the absolute value of H_E could decrease¹² or even more, it could change sign, as observed in previous works.²⁴ In Fig. 4, the solid line corresponds to a fit to Eq. (5) with J_i and N_v adjustable parameters, which indicates a quite good agreement of the experimental data with the simple model described above. Moreover, the agreement is not only qualitative but also quantitative. The exchange constant obtained from the fit was $J_i \approx -1.7$ meV. This coupling constant indicates an AFM coupling between the FM domains and the AFM host, explaining the tendency of M_E/M_S towards a reduction at high H_{cool} . On top of this, a mean field estimation of the exchange interaction for an antiferromagnet with $T_N = 155$ K gives $J \approx -1.8$ meV, in excellent agreement with the value obtained. This indicates that the exchange interaction within the AFM volume extends across the boundary with the FM domains without noticeable changes. Further, the number of spins per FM droplet is $N_v \approx 11$ ($\mu \approx 33 \mu_B$), corresponding to a droplet diameter $D \sim 10$ Å. This kind of FM nanodomain was already observed in the $\text{La}_{1-x}\text{Ca}_x\text{MnO}_3$ manganite²⁵ and in $\text{La}_{0.94}\text{Sr}_{0.06}\text{MnO}_3$,²⁶ where small angle neutron scattering experiments show the presence of FM droplets with the same characteristic size, and a density of domains $n \sim 10^{-5} \text{ \AA}^{-3}$. In our $\text{Pr}_{1/3}\text{Ca}_{2/3}\text{MnO}_3$ sample, an estimation of the density of FM droplets can be made from the saturation magnetization, which can be written as

$$M_S = n\mu \quad (6)$$

With $M_S \sim 2.8$ Gauss obtained from Fig. 2, we estimate $n \sim 0.9 \times 10^{-5} \text{ \AA}^{-3}$, which is very similar to the mentioned neutron scattering results. This density of droplets implies that the FM phase occupies only around 0.5% of the volume of the material, explaining the almost imperceptible FM signal that superposes on the AFM magnetization.

At this point it is worth noting that, although in previous works the small interface moment m_i has been detected by different techniques,^{3,4,5} in our case this moment is negligible as compared to M_E . An estimation from Eq. (3) indicates that the maximum contribution of the interface is $m_i \approx -0.027 \mu_B$ per surface spin. This represents only a 0.9% of the maximum possible value ($3 \mu_B$), in coincidence with measurements in other different systems.³ This m_i is indeed much smaller than the shift of the loops, which is $\sim 0.42 \mu_B$ per FM spin ($M_E/M_S \sim 0.14$) at the same cooling field. Moreover, while m_i is negative the measured M_E is always positive. Therefore, the magnetization shift measured in our system corresponds almost in its entirety to the remanence of the FM domains, as assumed in our analysis.

The exchange bias phenomenon observed in our material would be similar to that taking place in artificially fabricated nanocomposites,^{2,12,13,14,15} where FM nanoparticles are surrounded by the AFM oxide. This kind of core-shell interaction has been shown to provide quite strong magnetic anisotropies. In our case, using $M_E/M_S \sim 0.14$ and $H_E \sim -2$ kOe (for $H_{cool} = 70$ kOe), from Eq. (1) we can estimate an anisotropy constant $K \sim 3 \times 10^7$ erg/cm³. This is a quite important magnetic anisotropy, two orders of magnitude larger than the usual magnetocrystalline anisotropy measured in bulk FM manganites.²⁷ It is clear that this notable anisotropy constant is related to the particular magnetic configuration of the $\text{Pr}_{1/3}\text{Ca}_{2/3}\text{MnO}_3$ compound. In spring-magnet materials, it has been shown that the exchange anisotropy increases when the soft-FM domain size decreases, acquiring the anisotropy energy of the hard-FM matrix.^{10,11} Similarly, the exchange bias phenomenon is related to the surface exchange interaction between the FM and AFM phases. Therefore, it is widely accepted that, in nanocomposite materials, K is proportional to the surface-to-volume ratio of the FM domains. In the case of our nanometric FM domains, where $N_v \sim 11$, the ratio N_i/N_v is close to 1, being compatible with the high anisotropy constant estimated. Elastic effects in the charge-ordered phase tend to produce not spherical but elongated secondary phases,^{18,28} therefore a shape anisotropy energy could be also contributing to the anisotropy constant. From the structural point of view, the strength of the exchange anisotropy is influenced by the existence of surface strain and atomic displacement. This disorder modifies the interface exchange constant,^{6,8} and could be particularly relevant in nanocomposites where the constituents are structurally and chemically different. However, our manganite is an *intrinsic nanocomposite*, where the FM droplets appear naturally embedded in the AFM background and where structural and chemical differences should be less important. As a consequence, the obtained interface exchange constant is as large as in the bulk of the material, favoring a high exchange anisotropy as well.

C. Training effect

In exchange bias systems, a gradual decrease of the anisotropy interaction is commonly found as the material is continuously field-cycled; the so-called training effect.^{1,8,13,29,30,31} As a result, the exchange bias and the coercive fields decrease with increasing loop index number. In our manganite, the training effect is also present, as shown in Fig. 5. This figure presents the consecutive M^*-H loops measured for fields between 70 and -70 kOe, after the sample was field-cooled with $H_{cool} = 70$ kOe (only loops with index number $\lambda = 1, 2, 6,$ and 16 are shown). The relaxation of the magnetization shift is evident and, as shown by the evolution of M_E with λ (Fig. 6), this relaxation is particularly important between the

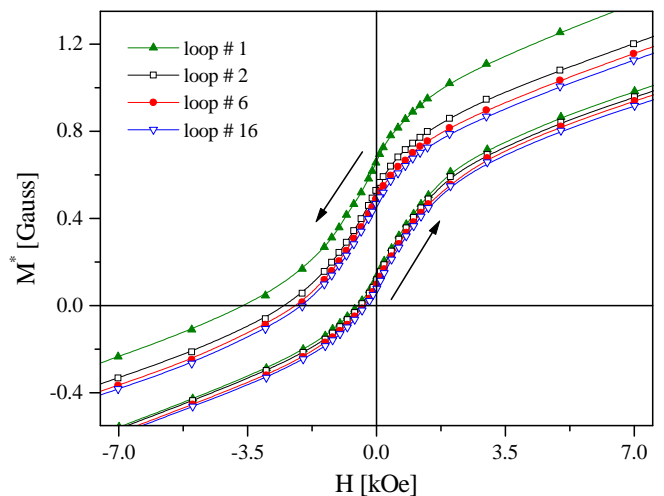


FIG. 5: Consecutive magnetization loops showing the training effect of the exchange bias. These data were measured after cooling the sample with $H_{cool} = 70$ kOe.

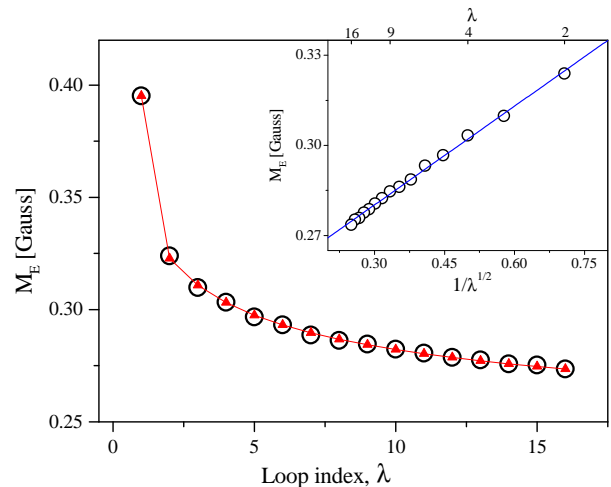


FIG. 6: The open circles are the experimental data of magnetization shift (M_E) vs loop index number (λ). The solid triangles correspond to a fit with a recursive law, that results from a discretized relaxation model. Inset: M_E vs $1/\sqrt{\lambda}$, showing the linear behavior usually obtained. The line is a least squares fit.

first and second loops, where M_E falls by $\sim 20\%$.

The training effect has been explained in terms of the demagnetization of the AFM surface moment m_i .^{13,29,31} As the FM domain switches back and forth under the influence of the applied field, a relaxation of the surface spin configuration towards the equilibrium is induced due to the *surface drag* of the exchange interaction. This is particularly relevant for glass-like phases, where multiple spin configurations are available. Indeed, it has been shown that magnetic frustration and the existence of

multiple easy axes orientations on the AFM counterpart of the FM/AFM interface are essential for the occurrence of training effects.³¹

The usual experimentally observed relationship between M_E and λ is given by

$$M_E(\lambda) - M_E^{eq} \propto \frac{1}{\sqrt{\lambda}} \quad (7)$$

where M_E^{eq} is the equilibrium magnetization shift. As shown in the inset of Fig. 6, this equation holds for $\lambda \geq 2$, with $M_E^{eq} = 0.247$ Gauss. However, as already stated in previous works²⁹ this equation holds only for loop indices $\lambda \geq 2$, and cannot explain the steep relaxation between the first and second loops. In recent work Binek,²⁹ using a discretized relaxation model deduced a recursive formula that relates the $(\lambda + 1)$ -th loop shift with the λ -th one as

$$M_E(\lambda + 1) = M_E(\lambda) - \gamma(M_E(\lambda) - M_E^{eq})^3 \quad (8)$$

with γ a sample dependent constant determined by microscopic parameters like the spin damping constant. With this simple relationship, and using $\gamma = 17.5$ Gauss⁻² and $M_E^{eq} = 0.235$ Gauss, the whole set of data is reproduced (solid triangles in Fig. 6), including the large initial drop of M_E . From Eq. (7), the recursive law is recovered for $\lambda \gg 1$, therefore explaining its applicability in this regime.

IV. CONCLUSIONS

In summary, we provide the first evidence of intrinsic interface exchange coupling in phase separated manganites. Our magnetization measurements show the coexistence of a predominant charge-ordered AFM phase and a minor FM component in the $\text{Pr}_{1/3}\text{Ca}_{2/3}\text{MnO}_3$ compound. Furthermore, after cooling the sample through the Néel temperature with an applied magnetic field this manganite presents exchange bias. This is clearly revealed by a distinctive magnetization shift (M_E) in the remanence of the M - H loops. The cooling field dependence of M_E at low temperature was successfully analyzed in terms of a simple exchange interaction model between FM nanodroplets of ~ 10 Å in size and a disordered (glassy-like) AFM shell. The observed training effect of the exchange bias can be described with the same relaxation model used for other classical exchange bias systems, indicating a similar mechanism for exchange anisotropy. Moreover, the anisotropy constant deduced, $K \sim 3 \times 10^7$ erg/cm³, is two orders of magnitude larger than the magnetocrystalline anisotropy of other common FM manganites. This large anisotropy energy opens a new possibility for the development of hard FM materials, where important exchange anisotropy interactions are introduced by intrinsic inhomogeneities that naturally occur in phase separated magnetic materials.

We acknowledge useful discussions with C. Leighton.

-
- ¹ For a review see, J. Nogués and I.K. Schuller, *J. Magn. Magn. Mater.* **192**, 203 (1999); and references therein.
- ² W.H. Meiklejohn and C.P. Bean, *Phys. Rev.* **102**, 1413 (1956); *ibid.* **105**, 904 (1957).
- ³ K. Takano, R.H. Kodama, A.E. Berkowitz, W. Cao, and G. Thomas, *Phys. Rev. Lett.* **79**, 1130 (1997).
- ⁴ A. Hoffmann, J.W. Seo, M.R. Fitzsimmons, H. Siegwart, J. Fompeyrine, J.-P. Locquet, J.A. Dura, and C.F. Majkrzak, *Phys. Rev. B* **66**, 220406(R) (2002).
- ⁵ W.J. Antel, Jr., F. Perjeru, and G.R. Harp, *Phys. Rev. Lett.* **83**, 1439 (1999); T.P.A. Hase, B.D. Fulthorpe, S.B. Wilkins, B.K. Tanner, C.H. Marrows, and B.J. Hickey, *Appl. Phys. Lett.* **79**, 985 (2001).
- ⁶ A.P. Malozemoff, *Phys. Rev. B* **37**, 7673 (1988); *J. Appl. Phys.* **63**, 3874 (1988).
- ⁷ D. Mauri, H.C. Siegmann, P.S. Bagus, and E. Kay, *J. Appl. Phys.* **62**, 3047 (1987).
- ⁸ J. Keller, P. Miltényi, B. Beschoten, G. Güntherodt, U. Nowak, and K.D. Usadel, *Phys. Rev. B* **66**, 014431 (2002).
- ⁹ K. Liu, S.M. Baker, M. Tuominen, T.P. Russell, and I.K. Schuller, *Phys. Rev. B* **63**, 060403(R) (2001); D.V. Dimitrov, S. Zhang, J.Q. Xiao, G.C. Hadjipanayis, and C. Prados, *ibid.* **58**, 12090 (1998).
- ¹⁰ R. Skomski and J.M.D. Coey, *Phys. Rev. B* **48**, 15812 (1993).
- ¹¹ L.H. Lewis, J.-Y. Wang, D.O. Welch, and V. Pan-
chanathan, *J. Appl. Phys.* **83**, 6274 (1998); P.G. McCormick, W.F. Miao, P.A.I. Smith, J. Ding, and R. Street, *ibid.* **83**, 6256 (1998).
- ¹² L. Del Bianco, D. Fiorani, A.M. Testa, E. Bonetti, and L. Signorini, *Phys. Rev. B* **70**, 052401 (2004).
- ¹³ R.K. Zheng, G.H. Wen, K.K. Fung, and X.X. Zhang, *Phys. Rev. B* **69**, 214431 (2004).
- ¹⁴ V. Skumryev, S. Stoyanov, Y. Zhang, G. Hadjipanayis, D. Givord, and J. Nogués, *Nature (London)* **423**, 850 (2003).
- ¹⁵ J. Löffler, H. Van Swygenhoven, W. Wagner, J. Meier, B. Doudin, and J.-Ph. Ansermet, *NanoStruct. Mater.* **9**, 523 (1997); Y.D. Yao, Y.Y. Chen, M.F. Tai, D.H. Wang, and H.M. Lin, *Mater. Sci. Eng. A* **217-218**, 281 (1996).
- ¹⁶ E. Dagotto, T. Hotta, and A. Moreo, *Phys. Rep.* **344**, 1 (2001).
- ¹⁷ D. Niebieskikwiat, R.D. Sánchez, L. Morales, and B. Maiorov, *Phys. Rev. B* **66**, 134422 (2002).
- ¹⁸ J. Tao, D. Niebieskikwiat, M.B. Salamon, and J.M. Zuo, *Phys. Rev. Lett.* **94**, 147206 (2005).
- ¹⁹ C.H. Chen, S-W. Cheong, and H.Y. Hwang, *J. Appl. Phys.* **81**, 4326 (1997).
- ²⁰ F. Nolting, A. Scholl, J. Stöhr, J.W. Seo, J. Fompeyrine, H. Siegwart, J.-P. Locquet, S. Anders, J. Lüning, E.E. Fullerton, M.F. Toney, M.R. Scheinfein, and H.A. Padmore, *Nature (London)* **405**, 767 (2000); H. Ohldag, A. Scholl, F. Nolting, S. Anders, F.U. Hillebrecht, and J. Stöhr, *Phys.*

- Rev. Lett. **86**, 2878 (2001).
- ²¹ R.H. Kodama, A.E. Berkowitz, E.J. McNiff, Jr., and S. Foner, Phys. Rev. Lett. **77**, 394 (1996).
- ²² H. Wang, T. Zhu, K. Zhao, W.N. Wang, C.S. Wang, Y.J. Wang, and W.S. Zhan, Phys. Rev. B **70**, 092409 (2004).
- ²³ C. Mitsumata, A. Sakuma, and K. Fukamichi, Phys. Rev. B **68**, 014437 (2003).
- ²⁴ J. Nogués, D. Lederman, T.J. Moran, and I.K. Schuller, Phys. Rev. Lett. **76**, 4624 (1996); J. Nogués, C. Leighton, and I.K. Schuller, Phys. Rev. B **61**, 1315 (2000).
- ²⁵ E. Granado, C.D. Ling, J.J. Neumeier, J.W. Lynn, and D.N. Argyriou, Phys. Rev. B **68**, 134440 (2003); M. Hennion, F. Moussa, G. Biotteau, J. Rodríguez-Carvajal, L. Pinsard, and A. Revcolevschi, Phys. Rev. Lett. **81**, 1957 (1998); M. Hennion, F. Moussa, J. Rodríguez-Carvajal, L. Pinsard, and A. Revcolevschi, Phys. Rev. B **56**, R497 (1997).
- ²⁶ M. Hennion, F. Moussa, G. Biotteau, J. Rodríguez-Carvajal, L. Pinsard, and A. Revcolevschi, Phys. Rev. B **61**, 9513 (2000).
- ²⁷ S.E. Lofland, S.M. Bhagat, C. Kwon, S.D. Tyagi, Y.M. Mukovskii, S.G. Karabashev, and A.M. Balbashov, J. Appl. Phys. **81**, 5737 (1997); F. Rivadulla, L.E. Hueso, C. Jardón, C. Vázquez-Vázquez, M.A. López-Quintela, J. Rivas, M.T. Causa, C.A. Ramos, and R.D. Sánchez, J. Magn. Magn. Mater. **196-197**, 470 (1999).
- ²⁸ V. Podzorov, B.G. Kim, V. Kiryukhin, M.E. Gershenson, and S-W. Cheong, Phys. Rev. B **64**, 140406(R) (2001)
- ²⁹ Ch. Binek, Phys. Rev. B **70**, 014421 (2004).
- ³⁰ A. Hochstrat, Ch. Binek, and W. Kleemann, Phys. Rev. B **66**, 092409 (2002).
- ³¹ A. Hoffmann, Phys. Rev. Lett. **93**, 097203 (2004).